Transient Resonance Raman and *ab Initio* MO Calculation Studies of the Structures and Vibrational Assignments of the T_1 State and the Anion Radical of Coumarin and Its Isotopically Substituted Analogues

Yuki Uesugi, Misao Mizuno, Atsuhiko Shimojima, and Hiroaki Takahashi*

Department of Chemistry, School of Science and Engineering, Waseda University, Tokyo 169, Japan

Received: August 30, 1996; In Final Form: October 28, 1996[⊗]

Transient resonance Raman and absorption spectra of the anion radical $CM^{\bullet-}$ and lowest excited triplet state $^3CM^*$ of coumarin were measured. Vibrational assignments of the ground state S_0, $CM^{\bullet-}$, and $^3CM^*$ were performed based on both the frequency shifts on isotopic (^{18}O, ^{13}C, and deuterium) substitutions and normal-coordinate calculations using the force constants obtained by *ab initio* molecular orbital computations. The vibrational assignments and *ab initio* MO calculations provided much information on the structures of S_0, $CM^{\bullet-}$, and $^3CM^*$. It is concluded that the C(3)═C(4) bond of the pyrone ring is lengthened markedly in $CM^{\bullet-}$ and drastically in $^3CM^*$. This suggests that the C(3)═C(4) bond is one of the reactive sites of coumarin and furocoumarins in their photochemical reactions, which is in good accord with the formation of cyclobutane-type adducts with pyrimidine bases, particularly with thymine, through the C(3)═C(4) bond of furocoumarins and the C(5)═C(6) bond of pyrimidine bases. The C═O bond was found to be moderately lengthened both in $CM^{\bullet-}$ and $^3CM^*$. The moderate lengthening of the C═O bond of $^3CM^*$ is consistent with the $\pi-\pi^*$ character of $^3CM^*$.

Introduction

Coumarin and its derivatives are known to exhibit photosensitizing properties. Particularly, furocoumarins (psoralen and its derivatives) have been reported to photoinduce skin erythema[1,2] and skin cancer in mice.[3] On the other hand, furocoumarins are important drugs used in the photochemotherapy of skin diseases such as psoriasis[4] and vitiligo.[5] The skin photosensitizing ability of furocoumarins has been correlated with their photoreactivity toward pyrimidine bases of DNA to form cyclobutane-type adducts and interstrand cross-links with two pyrimidine bases on separate strands of DNA double helix.[6,7]

In order to understand the photosensitizing mechanism of furocoumarins, it is important to obtain information on the structures and dynamics of the excited states and photolytically generated transient species of coumarin. Due to its structural similarities with psoralen, coumarin serves as a useful model for elucidating spectroscopic characteristics of the transient species of psoralen and its derivatives. In addition, coumarin itself is also known to show interesting photochemical behaviors, particularly the dimerization to form cis and trans head-to-head dimers through excited singlet and triplet states in polar and nonpolar solvents.[8] Studies on the structures of the photolytically generated transient species of coumarin may also provide important information on the reaction mechanism of this dimerization.

The purpose of this paper is to describe experimental and theoretical results on the structures and dynamics of the transient species involved in the photophysical and photochemical processes of coumarin obtained through nanosecond time-resolved absorption and resonance Raman spectroscopies and *ab initio* molecular orbital computations. Resonance Raman spectra of photoproduced transient species of coumarin including its electronic excited states have never been reported previously.

Experimental Section

Transient Raman spectra of the T_1 state $^3CM^*$ and anion radical $CM^{\bullet-}$ of coumarin were measured by the nanosecond time-resolved Raman spectroscopy system reported previously.[9] Briefly, an excimer laser (Lambda Physik LPX12Oi) was used as a light source for pumping, and an excimer-laser-pumped dye laser (FL3002E) was used as a light source for Raman probing. The energy of the excimer laser used for the pumping was about 100 mJ/pulse at the laser head and that of the dye laser used for Raman probing was 15−10 mJ/pulse at the laser head depending on the wavelength. The both lasers (pulse width, about 20 ns) were used at the repetition rate of 20 Hz. Nanosecond time-resolved absorption spectra were measured by a laser flash photolysis system constructed in our laboratory which consists of an excimer laser (Lambda Physik LPX12Oi) for pumping, a xenon lamp for white light, and a 30 cm spectrometer equipped with a gated multichannel detector.

Coumarin and DABCO (1,4-diazabicyclo[2.2.2]octane) were purchased from Kanto Chemical Co. Inc. and were used without further purification. Coumarin-^{18}O (carbonyl oxygen) was synthesized by the reaction of $H_2{}^{18}O$ (ISOTEC Inc., 97 atom %) with thiocoumarin[10] which was prepared by the reaction of coumarin with P_2S_5.[11,12] Coumarin-^{13}C (3-position of the pyrone ring) was synthesized by the reaction of salicylaldehyde with acetic anhydride-$^{13}C_2$ (carboxyl carbon atoms) (ISOTEC Inc., 99.2 atom %).[13] Coumarin-d_4 (phenyl group) was synthesized by the reaction of acetic anhydride with salicylaldehyde-d_4 (phenyl group) which was prepared by the reacton of phenol-d_6 (ISOTEC Inc., 99.2 atom %) with chloroform.[14]

Results and Discussion

Time-Resolved Absorption Spectra. Time-resolved absorption spectra of coumarin in deoxygenated ethanol measured by the nanosecond laser flash photolysis system are shown in Figure 1. The top figure (spectra a) represents the spectra of coumarin alone while the bottom figure (spectra b) represents those of coumarin with addition of an excess amount of DABCO. We have also measured the spectra in deoxygenated acetonitrile. The spectral time evolution in acetonitrile was almost the same as that in ethanol.

[⊗] Abstract published in *Advance ACS Abstracts,* December 15, 1996.

S1089-5639(96)02688-6 CCC: $14.00

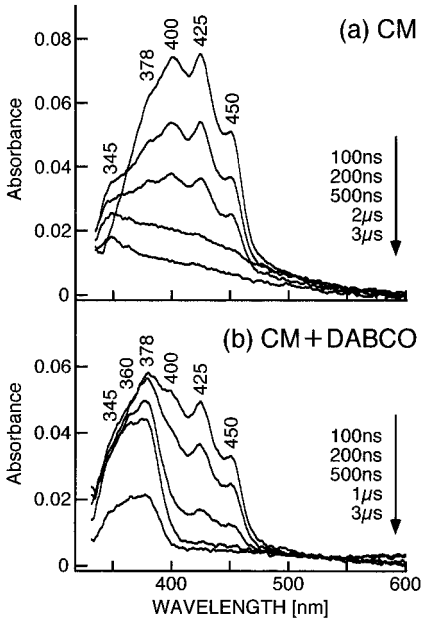

Figure 1. Time-resolved absorption spectra of coumarin in ethanol: (a) CM alone; from the top, measured 100 ns, 200 ns, 500 ns, 2 μs, and 3 μs after the pumping; (b) CM with addition of DABCO; from the top, 100 ns, 200 ns, 500 ns, 1 μs, and 3 μs after the pumping. Concentration of CM is 5.0×10^{-4} mol dm^{-3}. Concentration of DABCO is 5.0×10^{-3} mol dm^{-3}. Pump wavelength is 308 nm. Path length of the absorption cell is 0.25 cm.

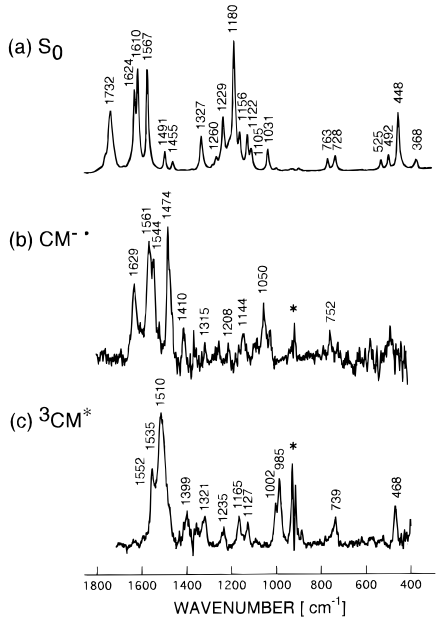

Figure 2. Raman spectrum of coumarin S_0 and transient resonance Raman spectra of $CM^{\bullet-}$ and $^3CM^*$ produced by irradiation with 308 num pump light: (a) S_0 in saturated acetonitrile solution; probe wavelength is 532 nm; (b) $CM^{\bullet-}$ in acetonitrile solution with the concentrations of CM and DABCO being 3.0×10^{-3} and 6.0×10^{-2} mol dm^{-3}, respectively; probe wavelength is 383 nm; (c) $^3CM^*$ in acetonitrile solution with the concentration being 3.0×10^{-3} mol dm^{-3}; probe wavelength is 420 nm. All spectra were measured at the pump−probe time delay of 100 ns. (*) Due to subtraction of solvent bands.

In the top figure three well-resolved peaks at 400, 425, and 450 nm and a shoulder at around 380 nm are seen at 100 ns after the pumping with 308 nm light. The shorter-wavelength side of this spectrum is obscured by the pump laser light. These peaks decrease in intensity with time and a band becomes apparent at 345 nm at around 2 μs. We observed that the peaks at 400, 425, and 450 nm were quenced drastically by the presence of oxygen. These peaks can be assigned to the T_1 state $^3CM^*$. The triplet state spectrum is in good agreement with that reported previously by Henry and Hunt[15] who showed that $^3CM^*$ exhibited three peaks at 406, 432, and 460 nm in EPA glass at 77 K. Land and Truscott,[16] however, reported a broad band at 395 nm for $^3CM^*$ in benzene at room temperature, and Chou et al.[17] reported a band at 465 nm for $^3CM^*$ in methylcyclohexane at room temperature.

In the bottom figure we see that the peak at 378 nm with a shoulder at around 360 nm is much stronger than that in the top figure. Since DABCO is a strong electron-donating agent and the $^3CM^*$ peaks at 400, 425, and 450 nm were quenched by the addition of DABCO, the 378 nm band with a shoulder at around 360 nm can be assigned to the anion radical $CM^{\bullet-}$ generated with $^3CM^*$ by obtaining an electron from the solvent (top case) or DABCO (bottom case). On the basis of the results of pulse radiolysis of coumarin in aqueous formate, Land and Truscott[16] assigned an absorption band around 360 nm to $CM^{\bullet-}$.

The intensity of the band at 345 nm appears to remain unchanged by the addition of DABCO. The identity of the 345 nm band is not certain but it is probable that this band arises from the cation radical $CM^{\bullet+}$ generated through the biphotonic process. The pump laser energy used in this measurement (100 mJ/pulse) may be sufficiently large for the biphotonic excitation. It is also probable that this band is attributable to a photolytically produced dimeric species.[8]

Raman Spectra of CM, $CM^{\bullet-}$, and $^3CM^*$ and Vibrational Assignments. In Figure 2 the resonance Raman spectrum of $CM^{\bullet-}$ measured with 383 nm probe light and the resonance Raman spectrum of $^3CM^*$ measured with 420 nm probe light are compared with the Raman spectrum of the ground state S_0 of coumarin measured with 532 nm probe light. Tamagake et al.[18] assigned the band at 1624 and 1180 cm^{-1} of the S_0 spectrum to the C(3)═C(4) stretch and C(2)−C(3) and/or C(4)−C(4a) stretch of the pyrone ring, respectively, based on Raman excitation profiles and PPP-CI molecular orbital calculations.

Vibrational assignments of other bands of S_0 and those of $CM^{\bullet-}$ and $^3CM^*$ have not been given before. However, comparison of these spectra reveals that the C═O stretch of $CM^{\bullet-}$ cannot be higher than 1629 cm^{-1} because no band is observed above this frequency. Also, the C═O stretch and pyrone C(3)═C(4) stretch of $^3CM^*$ cannot be higher than 1552 cm^{-1} because of the same reason. These results imply that the C═O bond is considerably weakened and therefore lengthened in $CM^{\bullet-}$ and much more lengthened in $^3CM^*$, and the C(3)═C(4) bond of $^3CM^*$ is also drastically lengthened. In order to obtain more detailed information on the structures of $CM^{\bullet-}$ and $^3CM^*$, accurate and reliable vibrational assignments are needed. For this purpose we have synthesized isotopicaly substituted analogues, i.e., CM-^{18}O (carbonyl oxygen), CM-^{13}C (3-position of the pyrone ring), and CM-d_4 (phenyl group) as shown in Figure 3, and measured the Raman or resonance Raman spectra of their ground states, anion radicals, and lowest excited triplet states to obtain frequency shifts on the isotopic substitutions.

Raman spectra of S_0 of the normal species (unsubstituted), CM-^{18}O, CM-^{13}C and CM-d_4 in acetonitrile are shown in Figure 4. It is seen that the band at 1732 cm^{-1} of the normal species is downshifted to 1706 cm^{-1} on the ^{18}O-substitution of the C═O group. The low-frequency shift of 26 cm^{-1} indicates that the 1732 cm^{-1} band can be assigned to the C═O stretch. The band at 1624 cm^{-1} appears to be downshifted to 1610 cm^{-1} on the ^{13}C substitution of the 3-position of the pyrone ring, overlapping with a band originally placed at this frequency. The low-frequency shift of 14 cm^{-1} is not sufficiently large to assign this band solely to the C(3)═C(4) stretch of the pyrone ring.

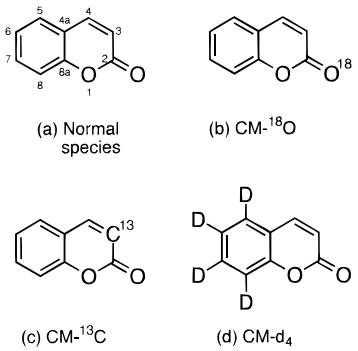

Figure 3. Structure and numbering system of coumarin and its isotopically substituted analogues studied.

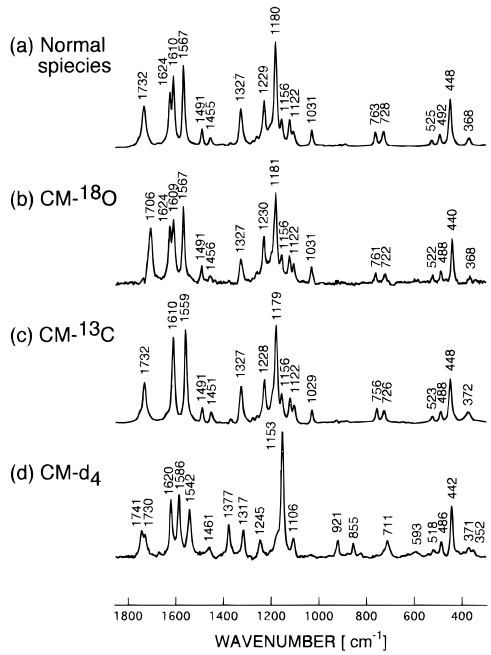

Figure 4. Raman spectra of the S_0 state of coumarin and its isotopically substituted analogues in acetonitrile (saturated solutions): (a) normal species; (b) CM-^{18}O; (c) CM-^{13}C; (d) CM-d_4. Probe wavelength is 532 nm.

This band should be considered to arise from a mixed mode of the C(3)═C(4) stretch and the phenyl 8a or 8b mode (Wilson vibration number[19]). This assignment is supported by the low-frequency shift of the band at 1567 cm^{-1} to 1559 cm^{-1} on the ^{13}C substitution. The 1567 cm^{-1} band should also be assigned to a mixed mode of the phenyl 8a or 8b mode (ring stretch) and the C(3)═C(4) stretch, probably the phase of mixing being opposite to that of 1610 cm^{-1}. The bands at 1610 and 1567 cm^{-1} are downshifted to 1586 and 1542 cm^{-1}, respectively, on the phenyl deuteration. The band at 1610 cm^{-1} can be assigned to the phenyl 8b mode (in disubstituted benzene 8b mode is usually higher than the 8a mode), and the above assignment of the band at 1567 cm^{-1} to a mixed mode of the 8a and C(3)═C-(4) stretch is now supported by this deuteration. The bands at 1491 and 1455 cm^{-1} are shifted to 1377 and 1317 cm^{-1} on the phenyl deuteration. These bands are assignable to the phenyl 19a and 19b modes (ring deformation + CH in-plane bend). It is seen that in the spectrum of CM-d_4 the C═O stretch band is split into a doublet at 1741 and 1730 cm^{-1}. This splitting is most probably caused by Fermi resonance between the C═O stretch and some overtone or combination band. Tamagake et al.[18] assigned the strong band at 1180 cm^{-1} to the C(2)−C(3) and/or C(4)−C(4a) stretch; however, this band does not involve contribution of the C(2)−C(3) stretch, because it does not exhibit

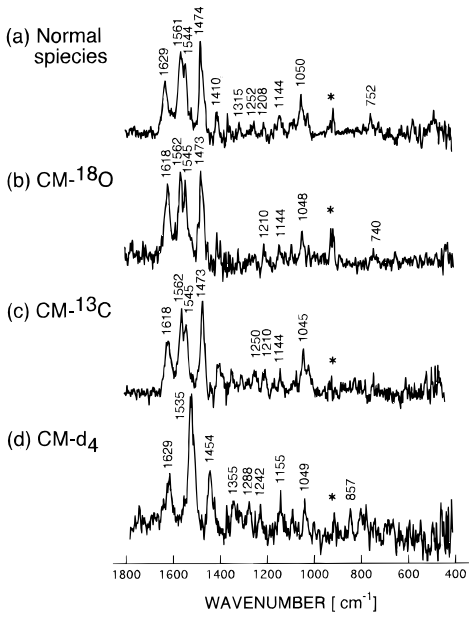

Figure 5. Transient resonance Raman spectra of CM$^{\bullet-}$ and its isotopically substituted analogues in acetonitrile: (a) normal species; (b) CM-^{18}O; (c) CM-^{13}C; (d) CM-d_4. Pump wavelength is 308 nm and probe wavelength is 383 nm. The pump−probe time delay is 100 ns for all spectra. Concentrations of CM and DABCO are 3.0×10^{-3} and 6.0×10^{-3} mol dm^{-3}, respectively. (*) Due to subtraction of solvent bands.

appreciable shifting on the ^{13}C substitution at the 3-position of the pyrone ring. Although the 1180 cm^{-1} band is downshifted to 1153 cm^{-1} on the phenyl deuteration, no phenyl vibrational mode is expected to exhibit such an isotopic frequency shift. This band is most probably attributable to a mode having a considerable contribution of the C−O stretch.

Transient resonance Raman spectra of the anion radical of the normal species, CM-^{18}O, CM-^{13}C, and CM-d_4 in acetonitrile are shown in Figure 5. The band at 1629 cm^{-1} is seen to be downshifted to 1618 cm^{-1} on the ^{18}O substitution. This band is also downshifted to 1618 cm^{-1} on the ^{13}C substitution. The downshift of only 11 cm^{-1} on the ^{18}O substitution with the same amount of the downshift on the ^{13}C substitution indicates that this band cannot be attributed to a pure C═O stretch but is a mixed vibrational mode of the C═O stretch and either the C(3)═C(4) or C(2)−C(3) stretch (since bond-order reversal is anticipated in anion radicals, it is not certain which bond has higher bond order). It is interesting to note that in the spectra of the anion radicals, the band attributable to the C(3)═C(4) stretch of the pyrone ring is not observable in the frequency region where double-bond stretches are expected to appear. We see that the band at 1050 cm^{-1} is shifted to 1045 cm^{-1} on the ^{13}C substitution. This band seems to be the only possible candidate assignable to the mode having appreciable contribution of the C(3)═C(4) stretch. This assignment implies that the bond order of the C(3)═C(4) bond is reduced to almost that of a single bond in CM$^{\bullet-}$. The bands at 1561 and 1544 cm^{-1} are downshifted to 1535 and 1523 cm^{-1} on the phenyl deuteration. These bands can be assigned to the phenyl 8b and 8a modes. We notice that the downshifts of 8b and 8a modes on going from S_0 (1610 and 1567 cm^{-1}) to CM$^{\bullet-}$ (1561 and 1544 cm^{-1}) are considerably large. This implies that the LUMO (lowest unoccupied molecular orbital) of CM involves significant contribution of π-electrons of the phenyl group. In other words, significant spin density is situated on the phenyl ring.

Transient resonance Raman spectra of the T_1 state of the normal species, CM-^{18}O, CM-^{13}C, and CM-d_4 in acetonitrile are shown in Figure 6. The band at 1552 cm^{-1} is downshifted

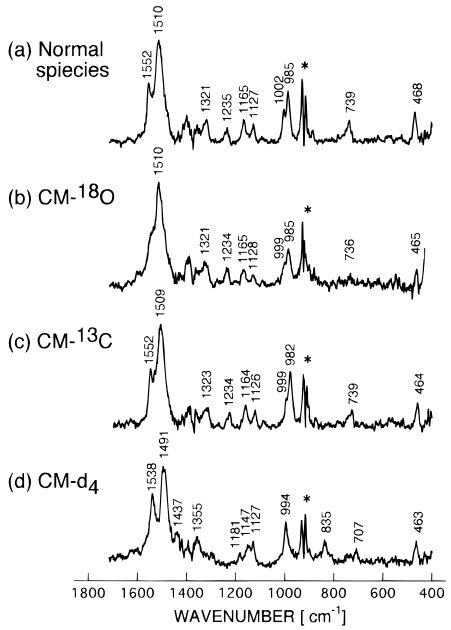

Figure 6. Transient resonance Raman spectra of ^{3}CM* and its isotopically substituted analogues in acetonitrile: (a) normal species; CM-^{18}O; (c) CM-^{13}C; (d) CM-d_4. Pump wavelength is 308 nm and probe wavelength is 420 nm. The pump−probe time delay is 100 ns for all spectra. Concentration is 3.0×10^{-3} mol dm^{-3}. (*) Due to subtraction of solvent bands.

to around 1537 cm^{-1} on the ^{18}O substitution (this band is more distinctly separated in ethanol solutions from the closely located band at 1510 cm^{-1}). The 1552 cm^{-1} band can be assigned to the C═O stretch. However, since this band also exhibits a shift of 14 cm^{-1} on the phenyl deuteration, more explicit characterization of this band is a mixed mode of the C═O stretch and the phenyl 8a or 8b mode. The moderate frequency decrease of the C═O stretch on going from S_0 (1732 cm^{-1}) to ^{3}CM* (1552 cm^{-1}) implies that ^{3}CM* is of a $\pi-\pi^*$ character.[20,21] The frequency decrease of a C═O stretch of the T_1 state having an $n-\pi^*$ character is expected to be much larger.[22] The $\pi-\pi^*$ character of the T_1 state of coumarin is in accord with the conclusion by Song and Gordon[23] and by Harrigan et al.[24] based on phosphorescence emission and excitation studies. The band at 1510 cm^{-1} is shifted to 1491 cm^{-1} on the phenyl deuteration. This band can be assigned to the phenyl 8a and 8b modes, possibly both being overlapped by each other. The large frequency decrease of the phenyl 8a and 8b modes on going from S_0 (1610 and 1567 cm^{-1}) to ^{3}CM* (1510 cm^{-1}) indicates that not only the LUMO but also the HOMO (highest occupied molecular orbital) must have a substantial contribution of π-electrons of the phenyl group. This means that the spin density on the phenyl ring is significantly large.

We note that no band assignable to the C(3)═C(4) stretch is observable in the frequency region of double-bond stretches. The spectrum of the ^{13}C-substituted analogue is almost identical to that of the normal species, except that the doublets at 1002 and 985 cm^{-1} are downshifted to 999 and 982 cm^{-1}, respectively. These results suggest that in ^{3}CM* the bond order of the C(3)═C(4) bond is decreased drastically to that of a single bond, and therefore, the C(3)═C(4) stretch is no longer a localized mode and is distributed over several vibrational modes (including those of the bands at 1002 and 985 cm^{-1}) in the frequency region of single-bond stretches.

Ab Initio MO Calculations of the Optimized Structures and Normal Frequencies. In order to obtain support for the vibrational assignments and the structures given above, *ab initio* molecular orbital calculations of the optimized structures and normal frequencies (in-plane vibrations only) of S_0 and CM$^{\bullet-}$ were carried out using the GAUSSIAN 94 packages of programs.[25] Calculations were performed at the RHF (restricted Hartree−Fock) level for S_0 and ROHF (restricted open-shell HF) level for CM$^{\bullet-}$ using the 4-31G (O*) basis set which includes polarization functions (d-orbitals) as the orbitals of oxygen atoms only. In the normal-coordinate calculations *ab initio* force constants were calculated first in terms of Cartesian displacement coordinates at the optimized geometry. They were then transformed into the force constants in terms of local symmetry coordinates consisting of symmetry coordinates of the phenyl moiety and internal coordinates of the pyrone moiety. Although this local symmetry coordinate system does not involve redundant coordinates of the phenyl ring, it still contains redundancy of the pyrone ring. Transformation of the Cartesian force constants into force constants in terms of the redundancy-containing local symmetry coordinates was performed using the method developed by Kuramshina et al.[26] The scaling of the force constants in terms of the local symmetry coordinates and internal coordinates was carried out according to the method reported in our preceding paper.[27] Briefly, the scale factors were transferred from structurally related simple molecules, the vibrational assignments of which had already been established.

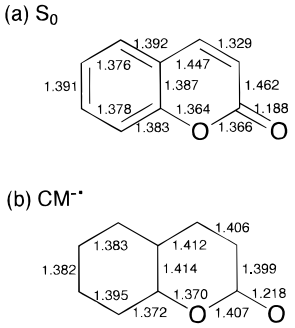

Figure 7. Structures of S_0 and CM$^{\bullet-}$: (a) optimized geometry of S_0 obtained by *ab initio* calculations at the RHF level using the 4-31G-(O*) basis set; (b) optimized geometry of CM$^{\bullet-}$ calculated at the ROHF level using the 4-31G(O*) basis set. (O*) represents the inclusion of polarization functions for oxygen atoms only. Both S_0 and CM$^{\bullet-}$ were calculated to be planar.

We have also calculated the structures and normal frequencies of ^{3}CM* at both the ROHF and UHF (unrestricted HF) levels. However, the ROHF-level calculations did not give $\pi-\pi^*$ character of the T_1 state, and due to spin contamination the UHF-level calculations were not considered to be reliable. These results are, therefore, not included in this paper. We believe that SCF-level calculations are not sugfficiently accurate for the electronic excited states, and in order to obtain reliable results, a calculation up to the DCI level is at least needed for taking electron correlation into account.

The optimized structures of S_0 and CM$^{\bullet-}$ are compared in Figure 7. The normal vibration frequencies of S_0 and CM$^{\bullet-}$ were obtained by using the force constants calculated at the optimized structures and are listed in Tables 1 and 2. The calculated structure of S_0 is quite consistent with the one expected from the Raman spectrum. The C═O bond length was calculated to be 1.188 Å, a value which indicates that the C═O bond is localized and is consistent with the Raman frequency 1732 cm^{-1}. The calculated C(3)═C(4) bond length 1.329 Å is indicative of an almost isolated C═C double bond and is again consistent with the Raman frequency 1624 cm^{-1}. The calculated normal frequencies are in good agreement with the observed and the vibrational assignments based on potential energy distributions (PED) support well the above empirical

TABLE 1: Observed and Calculated Normal Frequencies (cm^{-1})[a] of the S_0 States of Coumarin Normal Species, CM-^{18}O, CM-^{13}C, and CM-d_4, and the Potential Energy Distribution for the Normal Species

normal		CM-^{18}O		CM-^{13}C		CM-d_4		
obsd	calcd	obsd	calcd	obsd	calcd	obsd	calcd	assignment[b] PED (%)[c]
						1741		Fermi resonance
1732	1743	1706	1715	1732	1740	1730	1742	C═O str (86)
1624	1643	1624	1643	1610	1639	1620	1632	8a[d] (48); C(3)═C(4) str (16); CH (ph) ip bend (10)
1610	1621	1609	1618	1610	1616	1586	1601	8b (58); C(3)═C(4) str (12)
1567	1577	1567	1576	1559	1565	1545	1555	8a (31); C(3)═C(4) str (24); 8b (14)
1491	1489	1491	1489	1491	1489	1461	1429	CH (ph) ip bend (44); 19a (12)
1455	1451	1456	1450	1451	1447	1377	1386	CH (ph) ip bend (33); 19b (10)
e	1393		1392		1382		1336	CH (pyr) ip bend (58); CH (ph) ip bend (10)
1327	1334	1327	1334	1327	1334	1317	1321	14 (76); CH (ph) ip bend (12)
1276	1278	1276	1278	1276	1277		1031	CH (ph) ip bend (43)
1260	1265	1260	1264	1260	1265	1245	1245	C−O str (14); CH (pyr) ip bend (14)
1229	1224	1230	1224	1228	1222	1153	1154	C(4)−C(4a) str (16); 1 (15); CH (pyr) ip bend (15); CH (ph) ip bend (13)
1180	1213	1181	1213	1179	1212		1207	Ph−O str (34); CH (pyr) ip bend (17); C(2)−C(3) str (11)
1156	1162	1156	1162	1156	1162		821	CH (ph) ip bend (69)
1122	1124	1122	1124	1122	1122		836	CH (ph) ip bend (33); CH (pyr) ip bend (10)
1105	1100	1105	1099	1105	1099	1106	1104	CH (pyr) ip bend (35); 12 (15); CH (ph) ip bend (11)
1031	1022	1031	1022	1029	1022	855	847	1 (26); CH (ph) ip bend (18)
	921		915		919	921	913	12 (32); Ph−O str (12); C(2)−C(3) str (10)
891	888		888		881		874	12 (18); ring (pyr) def (29); C−O str (11)
763	750	761	750	756	746	711	712	1 (20); 6b (20); C(4)−C(4a) str (12); ring (pyr) def (10)
728	727	722	720	726	725		706	6a (20); C(2)−C(3) str (11)
	607		605		606	593	596	6a (31); 6b (24); C═O ip bend (12)
525	525	522	523	523	523	518	518	6a (40); C═O ip bend (16)
492	478	488	473	488	474	486	470	C═O ip bend (37); ring (pyr) def (60)
448	439	440	431	448	438	442	431	ring (pyr) def (45); 6a (10)
	300		294		299		287	ring (pyr) def (38); 6a (16); C═O ip bend (15)

[a] Only in-plane vibrations are shown. [b] C−H stretches are not shown. str, def, ip, ph, and pyr denote stretch, deformation, in-plane, phenyl, and pyrone, respectively. [c] Contributions less than 10% are not given. [d] Phenyl vibration numbers are due to Wilson.[19] 1, ring breathe; 6a, 6b, ring deformation; 8a, 8b, ring stretch; 12, trigonal vibration; 14, Kekulé vibration; 19a, 19b, ring deformation + CH in-plane bend. [e] Denotes not observed.

TABLE 2: Observed and Calculated Normal Frequencies (cm^{-1})[a] of the Anion Radical of Coumarin Normal Species, CM-^{18}O, CM-^{13}C, and CM-d_4, and the Potential Energy Distribution for the Normal Species

normal		CM-^{18}O		CM-^{13}C		CM-d_4		
obsd	calcd	obsd	calcd	obsd	calcd	obsd	calcd	assignment[b] PED (%)[c]
1629	1639	1618	1628	1618	1631	1629	1637	C═O str (51); C(2)−C(3) str (21)
1561	1578	1562	1577	1562	1577	1535	1547	8b[d] (70); CH (ph) ip bend (13)
1544	1557	1545	1552	1545	1557	1523	1537	8a (60); C═O str (18); CH (ph) ip bend (12)
1474	1477	1473	1475	1473	1475	*e*	1318	CH (ph) ip bend (28)
	1466		1464		1464	1454	1452	C(2)−C(3) str (23); CH (ph) ip bend (15)
1410	1408		1407		1406		1409	CH (ph) ip bend (34); CH (pyr) ip bend (13); C(3)═C(4) str (11)
	1356		1350		1339	1355	1350	CH (pyr) ip bend (61); C═O str (10)
1315	1318		1318		1317	1288	1287	14 (79); CH (ph) ip bend (10)
	1264		1264		1264		1123	CH (pyr) ip bend (16); CH (ph) ip bend (14)
1252	1261		1260	1250	1259	1242	1251	CH (ph) ip bend (16); C−O str (13); CH (pyr) ip bend (12); 12 (10)
1208	1218	1210	1218	1210	1217	1155	1160	Ph−O str (14); 1 (11); CH (ph) ip bend (10); CH (pyr) ip bend (10)
1144	1151		1150	1144	1150		1021	CH (ph) ip bend (51)
	1138		1137		1135		814	CH (ph) ip bend (20); C(4)−C(4) str (15); Ph−O str (14); 12 (12)
	1989		1089		1088		878	CH (ph) ip bend (32); 12 (14)
1050	1033	1048	1032	1045	1028	1049	1030	CH (pyr) ip bend (33); C(3)═C(4) str (18); Ph−O str (11); C═O ip bend (10)
	1019		1019		1018	857	863	1 (19); CH (ph) ip bend (17)
	877		877		872		841	C−O str (17); 12 (14); Ph−O str (12)
	863		860		862		805	Ph−O str (29); 12 (28)
752	744	740	743		739		709	1 (24); 6b (13); ring (pyr) def (13)
	724		716		722		701	6a (15); ring (pyr) def (12)
	605		603		604		592	6b (38); 6b (23); C═O ip bend (14)
	530		526		528		522	6b (44); C═O ip bend (21)
	461		458		457		454	C═O ip bend (31); ring (pyr) def (59)
	432		425		431		425	ring (pyr) def (56)
	296		290		296		284	ring (pyr) def (33); 6a (15); 6b (13); C−O str (10)

[a] Only in-plane vibrations are shown. [b] C−H stretches are not shown. str, def, ip, ph, and pyr denote stretch, deformation, in-plane phenyl, and pyrone, respectively. [c] Contributions less than 10% are not given. [d] Phenyl vibration numbers are due to Wilson.[19] 1, ring breath; 6a, 6b, ring deformation; 8a, 8b, ring stretch; 12, trigonal vibration; 14, Kekulé vibration; 19a, 19b, ring deformation + CH in-plane bend. [e] Denotes not observed.

assignments based on the isotopic frequency shifts. The contribution of the C═O stretch to the 1732 cm^{-1} band was calculated to be 86% in good agreement with the large ^{18}O-frequency shift of 26 cm^{-1}, and the 1624 cm^{-1} band was calculated to involve substantial contributions of both the phenyl 8a and C(3)═C(4) stretch. As was predicted above, the 1180 cm^{-1} band was calculated to have largest contribution of the C−O stretch.

The optimized geometries of $CM^{\bullet-}$ is quite interesting and suggestive. The C═O bond length was calculated to be 1.218 Å, a value which is longer by 0.03 Å than the C═O bond length of S_0. The lengthening of 0.03 Å of the C═O bond may be considered to be in accord with the relatively small downshift (103 cm^{-1}) of the C═O stretch on going from S_0 to $CM^{\bullet-}$. The calculated C(3)═C(4) bond length of 1.406 Å indicates that the bond order of the C(3)═C(4) bond is greatly decreased and is in good accord with the experimental result that no band assignable to the C(3)═C(4) stretch is observed in the double-bond-stretch region. The C(2)−C(3) and C(4)−C(4a) bond lengths were calculated to be 1.399 and 1.412 Å, respectively, indicating that the bond order of these two bonds is greatly increased. The decrease of the bond order of the C(3)═C(4) double bond and the increase of the bond orders of the C(2)−C(3) and C(4)−C(4a) single bonds indicate that bond order reversal is occurring in the pyrone ring of $CM^{\bullet-}$.

The bond order reversal in $CM^{\bullet-}$ may be interpreted in terms of HOMO−LUMO considerations. Since the electronic state of $CM^{\bullet-}$ can most adequately be approximated by the electronic configuration in which the HOMO is filled up and an additional electron occupies the LUMO. Thus the nature of $CM^{\bullet-}$ is mainly governed by the nature of the LUMO. It is reasonable to consider that the LUMO has antibonding nature with respect to the π-bonding of the C(3)═C(4) double bond. Thus, the addition of an electron to the LUMO leads to the lengthening of the C(3)═C(4) bond. On the other hand, the LUMO has bonding nature with respect to the π-bonding of the C(2)−C(3) and C(4)−C(4a) single bonds. Therefore, the addition of an electron to the LUMO leads to the shortening of these bonds.

The calculated normal frequencies of $CM^{\bullet-}$ using the *ab initio* force constants calculated at the optimized geometry are in good agreement with the observed (Table 2). The PEDs clearly show that the contribution of the C(3)═C(4) stretch of the pyrone ring is not localized into a single vibrational mode but is distributed over several modes with the calculated frequencies 1033 (PED 18%), 1408 (11%), 1477 (8%), 1466 (7%), 1356 (7%), and 1639 cm^{-1} (6%) (contributions less than 10% are not given in Table 2). The 1474 cm^{-1} band was calculated to have the largest contribution from the C(2)−C(3) stretch (PED 23%), indicating that the double-bond nature of the C(2)−C(3) bond is quite large. The calculations also show that the downshift (−11 cm^{-1}) of the 1629 cm^{-1} band on the ^{13}C substitution is due to the contribution of the C(2)−C(3) stretch (PED) 21%) and not of the C(3)═C(4) stretch.

Although optimized geometry of $^3CM^*$ was not obtained, more pronounced bond order reversal is expected to occur in $^3CM^*$. The electronic state of $^3CM^*$ is most adequately approximated by the electronic configuration in which an electron is elevated from the HOMO to the LUMO. Since the HOMO has bonding nature and LUMO has antibonding nature with respect to the π-bonding of the C(3)═C(4) double bond, the removal of an electron from the HOMO lengthens the C(3)═C(4) bond and the addition of this electron to the LUMO further lengthens the bond. On the contrary, the HOMO has antibonding nature and LUMO has bonding nature with respect to the C(2)−C(3) and C(4)−C(4a) single bonds. Therefore, the removal of an electron from the HOMO shortens these bonds and the addition of this electron to the LUMO further shortens these bonds. This prediction is in good accord with the experimental results that no band assignable to the C(3)═C(4) stretch is detectable in the double-bond-stretch region and the contribution of the C(3)═C(4) stretch is distributed over vibrational modes in the single-bond stretch region.

Conclusions

We have shown by time-resolved resonance Raman spectroscopy and *ab initio* MO calculations that bond order reversal occurs in the pyrone moiety of coumarin in both the anion radical $CM^{\bullet-}$ and lowest excited triplet state $^3CM^*$. The C(3)═C(4) bonds of these transients are drastically lengthened out into an almost single bond, with concomitant shortening of the C(2)−C(3) and C(4)−C(4a) bonds. This indicates that the C(3)═C(4) bond is one of the reactive sites of coumarin and furocoumarins in their photochemical reactions, and provides strong support to the previous reports that on irradiation with near UV light, furocoumarins form cycloadducts with pyrimidine bases, particularly with thymine, through the C(3)═C(4) bond of furocoumarins and the C(5)═C(6) bond of pyrimidine bases.[6,7]

The C═O stretch of the pyrone moiety was observed 1732, 1629, and 1552 cm^{-1} for S_0, $CM^{\bullet-}$, and $^3CM^*$, respectively. Although the contribution of the C═O stretch to these bonds decreases as the frequency decreases, the frequency decrease on going from S_0 to $CM^{\bullet-}$ and to $^3CM^*$ indicates that the C═O bond lengthens in this order. The C═O stretching frequency of 1552 cm^{-1} of $^3CM^*$ indicates that the C═O bond still retains double bond nature considerably and $^3CM^*$ is of the $\pi-\pi^*$ character. This also suggests that the C═O bond may not be the reactive site of coumarin and furocoumarins both for the anion radical and T_1 state.

The frequencies of the 8b and 8a modes decrease on going from S_0 (1610 and 1567 cm^{-1}) to $CM^{\bullet-}$ (1561 and 1544 cm^{-1}) and to $^3CM^*$ (1510 cm^{-1}, 8a and 8b overlapping each other). Since the bands at 1610 (S_0), 1561 ($CM^{\bullet-}$), and 1510 cm^{-1} ($^3CM^*$) do not involve the contribution of the C(3)═C(4) or C(2)−C(3) stretch and the contribution of the 8b mode is quite large, these frequency decreases may be considered to indicate that the phenyl ring is softened in this order. This means that although both the HOMO the LUMO involve very large contribution of π-electrons of the pyrone moiety as evidenced by the very large low-frequency shifts of the C(3)═C(4) and C═O stretches, the contribution of π-electrons of the phenyl group is also significant.

Acknowledgment. The authors are grateful to Advanced Research Institute for Science and Engineering Waseda University for financial support.

References and Notes

(1) Patak, M. A.; Fellman, J. H.; Kaufman, K. D. *J. Invest. Dermatol.* **1960**, *35*, 165.
(2) Musajo, L. *Ann. Ist. Super. Sanita* **1969**, *5*, 376.
(3) Giese, A. C. *Photophysiology* **1971**, *6*, 77.
(4) Parrish, J. A.; Fitzpatrick, T. B.; Tannenbaum, L.; Patak, M. A. *New Engl. J. Med.* **1974**, *291*, 1207.
(5) Fitzpatrick, T. B.; Parrish, J. A.; Pathak, M. A. In *Sunlight and Man*; Patak, M. A., Harber, C., Seiji, M., Kurita, A., Eds.; University of Tokyo Press: Tokyo, 1974; p 783.
(6) Dall'Acqua, F.; Marciani, S.; Ciavatta, L.; Rodighiero, G. *Z. Naturforsch.* **1971**, *26b*, 561.
(7) Musajo, L.; Rodighiero, G. *Photophysiology* **1972**, *7*, 115.
(8) Hammond, G. S.; Stout, C. A.; Lamola, A. A. *J. Am. Chem. Soc.* **1964**, *86*, 3103.
(9) Hashimoto, S.; Shimojima, A.; Yuzawa, T.; Hiura, H.; Abe, J.; Takahashi, H. *J. Mol. Struct.* **1991**, *242*, 1.
(10) Jorgensen, K. A.; Ghattas, A.-B. A. G.; Lawesson, S.-O. *Tetrahedron* **1982**, *38*, 1163.
(11) Devanathan, S.; Ramamuthy, V. *J. Org. Chem.* **1988**, *53*, 741.
(12) Becker, R. S.; Chakravorti, S.; Gartner, A. *J. Chem. Soc., Faraday Trans.* **1993**, *89*, 1007.
(13) Simandan, T. L. Rom. RO94549(CI.C07D311/06), 15 Aug. 1988, Appl. 124889, 01 Oct. 1986.
(14) Thoer, A.; Denis, G.; Delmas, M.; Gaset, A. *Synth. Commun.* **1988**, *18*, 2095.

(15) Henry, B. R.; Hunt, R. V. *J. Mol. Spectrosc.* **1971**, *39*, 466.
(16) Land, E. J.; Truscott, T. G. *Photochem. Photobiol.* **1979**, *29*, 861.
(17) Chou, P.-T.; Martinez, M. L.; Studer, S. L. *Chem. Phys. Lett.* **1992**, *188*, 49.
(18) Tamagake, K.; Tsuboi, M.; Nakamoto, K. In *Time-Resolved Vibrational Spectroscopy V*; Takahashi, H., Ed.; Springer-Verlag: Berlin, 1991; p 161.
(19) Wilson, Jr., E. B. *Phys. Rev.* **1934**, *45*, 706.
(20) Tahara, T.; Hamaguchi, H.; Tasumi, M. *J. Phys. Chem.* **1990**, *94*, 170.
(21) Ebihara, K.; Hiura, H.; Takahashi, H. *J. Phys. Chem.* **1992**, *96*, 9120.
(22) Tahara, T.; Hamaguchi, H.; Tasumi, M. *J. Phys. Chem.* **1987**, *91*, 5875; *Chem. Phys. Lett.* **1988**, *152*, 135.
(23) Song, P.-S.; Gordon, W. H. *J. Phys. Chem.* **1970**, *74*, 4234.
(24) Harrigan, E. T.; Chakrabarti, A.; Hirota, N. *J. Am. Chem. Soc.* **1976**, *98*, 3460.
(25) Carnegie-Mellon Quantum Chemistry Publishing Unit, Pittsburgh, PA, 1994.
(26) Kramshina, G. M.; Weinhold, F.; Kochikov, I. V.; Yagola, A. G.; Pentin, Yu. A. *J. Chem. Phys.* **1994**, *100*, 1414.
(27) Shimojima, A.; Takahashi, H. *J. Phys. Chem.* **1993**, *97*, 9103.